AIP Advances

The potential application of ultra-nanocrystalline diamond films for heavy ion irradiation detection

Huang-Chin Chen, Shih-Show Chen, Wei-Cheng Wang, Chi-Young Lee, Jinghua Guo, I-Nan Lin, and Ching-Lin Chang

Citation: AIP Advances **3**, 062113 (2013); doi: 10.1063/1.4811338
View online: http://dx.doi.org/10.1063/1.4811338
View Table of Contents: http://scitation.aip.org/content/aip/journal/adva/3/6?ver=pdfcov
Published by the AIP Publishing

AIP ADVANCES **3**, 062113 (2013)

The potential application of ultra-nanocrystalline diamond films for heavy ion irradiation detection

Huang-Chin Chen,[1,3] Shih-Show Chen,[1,2] Wei-Cheng Wang,[1]
Chi-Young Lee,[3] Jinghua Guo,[4] I-Nan Lin,[1,a] and Ching-Lin Chang[1,a]
[1]*Department of Physics, Tamkang University, Tamsui, New-Taipei, Taiwan 251, ROC*
[2]*Department of Information Technology and Mobile Communication, Taipei College of Maritime Technology, Tamsui, New-Taipei, Taiwan 251, ROC*
[3]*Department of Materials Science and Engineering, National Tsing Hua University, Hsinchu, Taiwan, 300, ROC*
[4]*Advanced Light Source, Lawrence Berkeley National Laboratory, Berkeley, CA 94720, USA*

(Received 22 March 2013; accepted 3 June 2013; published online 11 June 2013)

The potential of utilizing the ultra-nanocrystalline (UNCD) films for detecting the Au-ion irradiation was investigated. When the fluence for Au-ion irradiation is lower than the critical value ($f_c = 5.0 \times 10^{12}$ ions/cm^2) the turn-on field for electron field emission (EFE) process of the UNCD films decreased systematically with the increase in fluence that is correlated with the increase in sp^2-bonded phase (π^*-band in EELS) due to the Au-ion irradiation. The EFE properties changed irregularly, when the fluence for Au-ion irradiation exceeds this critical value. The transmission electron microscopic microstructural examinations, in conjunction with EELS spectroscopic studies, reveal that the structural change preferentially occurred in the diamond-to-Si interface for the samples experienced over critical fluence of Au-ion irradiation, viz. the crystalline SiC phase was induced in the interfacial region and the thickness of the interface decreased. These observations implied that the UNCD films could be used as irradiation detectors when the fluence for Au-ion irradiation does not exceed such a critical value. [http://dx.doi.org/10.1063/1.4811338]

I. INTRODUCTION

Diamond films have been extensively investigated for the application as radiation detectors,[1–4] since these materials exhibit extreme resilience to harsh environments, in comparison to other semiconducting materials. However, the hydrogen retention in the microcrystalline diamond (MCD) films during the growth of the films can markedly alter the bonding,[5–7] conductivity[8] and field emission[9] of diamond films. The change in electrical properties of MCD films due to heavy ion irradiation will be affected by the hydrogen content in the diamond that results in some ambiguity in radiation detection, as the control of hydrogen content in the diamond films is difficult. Moreover, the MCD films are susceptible to the induction of structural defects due to heavy ion irradiation[10] that is detrimental to the application of these materials as a radiation detector. Such a phenomenon is due to the fact that the principle of radiation detection in diamond relies on the measurement of electron-hole pairs created within the diamond during the interaction of the incident particles or photons to be detected. When structural defects are induced by heavy ion irradiation, the presence of point defects (vacancies) in a semiconductor will lower the mobility of the electrons through the impurity scattering mechanism[11] and that of line defects (dislocations) will act as electron traps that lower the conductivity of the materials by decreasing in electron concentration.[11]

[a]Corresponding author, e-mail: inanlin@mail.tku.edu.tw (I-Nan Lin); clchang@mail.tku.edu.tw (Ching-Lin Chang)

Ultra-nanocrystalline diamond (UNCD) film has recently attracted significant attention from researchers because of its unique granular structure,[12] viz. the grains of UNCD films have an sp^3 character, the grain-boundaries have a mixture of sp^2, sp^3, hydrocarbon and amorphous carbon, in which the sp^2 character is predominant.[13,14] This material shows better potential for application as a radiation detector, as the conductivity of the pristine UNCD films can be reliably controlled by carefully adjusting the granular structure of diamond films. Many reports have discussed the effects of ion beam irradiation on the characteristics of diamond and related materials, such as type IIa diamond,[15] diamond-like carbon films,[16] taC,[17] graphite[18] and polycrystalline CVD diamond films.[19–21] Especially, Pandey *et al*.[22] and Koinkar *et al*.[23] have studied the field emission enhancement by swift heavy ion irradiation in CVD diamonds.

In this article, we reported the effect of heavy-ion (2.245 GeV Au) irradiation on altering the electron field emission (EFE) properties of UNCD films so as to understand the feasibility of using these materials as radiation detectors. The modifications to the bonding structure of these films due to heavy ion irradiation were investigated in detail by near edge x-ray absorption fine structure spectroscopy (NEXAFS) and electron energy loss spectroscopy (EELS). The modification on the granular structure of these films due to heavy ion irradiation was examined using transmission electron microscopy (TEM). The change in EFE properties of these films was correlated with the modification on the granular structure of the films to understand the related mechanism.

II. EXPERIMENTAL PROCEDURES

The UNCD films were deposited via microwave plasma enhanced chemical vapor deposition (MPECVD) processing using a cylindrical reactor (Innovative Plasma Systems GmbH, CYRANNUS-I). Prior to the deposition of diamond films, the silicon substrates were ultrasonicated in methanol solution, containing nano-diamond powder (∼5 nm) and titanium powder, for 45 minutes to create nucleation sites. In the growth of diamond films, a gas mixture of CH_4 and Ar with flow rates of 1 and 99 sccm, respectively, was excited by 1200 W microwave radiation at 2.45 GHz, and the total pressure in the chamber was maintained at 100 torr. The substrate temperature was estimated to be around 475°C during the growth of the UNCD films. The film thickness was estimated by cross-sectional scanning electron microscopic observation to be around 300 nm with the growth time of 60 minutes for each film.

The UNCD diamond films were subjected to 2.245 GeV Au-ion irradiation from the Universal Linear Accelerator (UNILAC) at GSI Helmholtzzentrum für Schwerionenforschung GmbH, Darmstadt, Germany. The ion flux of Au for irradiating the diamond films is around 9.3×10^8 ions/cm$^2 \cdot$ s over an area about 0.5 cm^2. The 2.245 GeV gold ions have a projected range of 66.4 μm in diamond with longitudinal straggling of 1.93 μm as simulated with SRIM-2008.[24] Therefore, the Au-ions will pass through the diamond films and get buried deep in the substrate for all the samples. There is no doping effect due to the Au-ion irradiation. The Au-ions have an electronic energy loss of 3.34×10^4 eV/nm and a nuclear energy loss of 28.99 eV/nm, which indicates that the ions will lose energy mostly through electronic excitations in the diamond. The lattice damage effects of nuclear energy loss will be minimal. The annealing process was conducted in a 5% H_2/Ar atmosphere at 1000°C for 1 hour. The pristine UNCD samples were designated as samples f_0. The samples exposed to Au-ion irradiated with fluences of $f_a = 1 \times 10^{11}$, $f_b = 1 \times 10^{12}$, and $f_c = 5 \times 10^{12}$ ions/cm^2 were designated as samples f_a, f_b and f_c, respectively, and the corresponding samples, which were annealed after the Au-ion irradiation were designated as samples f_{aa}, f_{ba} and f_{ca}, respectively.

The films were characterized using scanning electron microscopy (SEM: JEOL JSM-6500F), Raman spectroscopy (Renishaw, excitation wavelength = 514.5 nm) and transmission electron microscopy (Jeol 2100). The detailed microstructure and bonding structure of the samples were examined using electron energy loss spectroscopy (EELS, Gatan Enfina) in transmission electron microscopy. The C*1s* near edge x-ray absorption fine structure (NEXAFS) measurements were carried out at the Lawrence Berkeley National Laboratory (LBNL), Advanced Light Source (ALS) at beamline 7.0.1. The beamline is equipped with a 99-pole, 5-cm period undulator and spherical grating monochromator. The NEXAFS spectra were obtained in the total electron yield mode by measuring the photocurrent directly from the sample. All the samples measured are conducting reasonably

well, thus no sample charging effect was observed during the experiments. The resolutions were set to 0.1 eV at 290 eV (in the vicinity of the C*1s* edge). A piece of highly oriented pyrolitic graphite sample was used as the standard samples for energy calibration. The EFE properties of the samples were measured using a parallel setup. The anode (W-rod, 1 mm in diameter) was separated from the cathode, on which our samples were attached, with the cathode-to-anode distance controlled by an adjustable micrometer attached to the anode. The current-to-voltage characteristics of the UNCD-coated Si-templates were acquired using a Keitheley 237 electron source meter, in a high vacuum environment (5×10^{-6} torr). The current density vs. applied field *(J-E)* curves were modeled by Fowler-Nordheim (F-N) model.[25] The turn-on field for inducing the EFE process was designated as the interception of the lines extrapolated from the low-field and high-field segments in F-N plots, which were in $J/E^{2\ \text{vs.}\ 1/E}$ curves.

III. RESULTS

A. The overall Au-ion irradiation effect

For an ideal heavy ion irradiation detector, the detectable electronic properties of the materials should change with the fluence of ion irradiation systematically and the structural damage induced by the irradiation should be minimized. Figure 1 shows the modification on SEM morphology of UNCD films due to Au-ion irradiation and the irradiation/annealing processes. The pristine UNCD films contain small grain micrstructue (Fig. 1(a)). The Au-ion irradiation (Figs. 1(b_i), 1(c_i), and 1(d_i)) and the followed annealing processes (Figs. 1(b_{ii}), 1(c_{ii}), and 1(d_{ii})) hardly altered the granular structure of the UNCD films. Only grooving along the aggregates of diamond films was observable. Figures 2(a) and 2(b) show the modification on Raman spectroscopy due to Au-ion irradiation and the irradiation/annealing processes, respectively. The Raman spectrum of the pristine UNCD films contains very broaden Raman resonance peaks (curve i, Fig. 2(a)) that is the characteristics of the diamond films with ultra-small grains.[26] There exists ν_1-band (1140 cm^{-1}) and ν_3-band (1480 cm^{-1}), which represents transpoly-acetylene phase located at the grain boundaries of the UNCD films. There also presents the D*-band (1350 cm^{-1}) and G*-band (1580 cm^{-1}), which represents the disordered carbon and graphitic phases. Figure 2(b) shows that the annealing process after Au-ion irradiation do not markedly change such characteristics.

While Figs. 1 and 2 reveal that the SEM morphologies and the Raman spectroscopy of the UNCD films are hardly altered due to the Au-ion irradiation and the irradiation/annealing processes, Figs. 3(a) and 3(b) show that the EFE properties of the films change systematically with the fluence of Au-ion irradiation and the irradiation/annealing processes, respectively. These figures indicate that the EFE process of the pristine UNCD films can be turned on at 30 V/μm, and reach a current density of about 0.4 mA/cm^2 at an applied field of 100 V/μm (curve I). The turn-on field decreases monotonously with the fluence of Au-ion irradiation for the irradiation fluence up to $f_b = 1 \times 10^{12}$ ions/cm^2. Whereas the turn-on field reverted back to larger value for the samples f_c (curve IV), which was irradiated with critical fluence of $f_c = 5 \times 10^{12}$ ions/cm^2. The variation of the turn-on field as a function of the ion dosage is plotted as solid squares in Fig. 3(c). The irradiation/annealing process slightly modified the EFE properties of the samples. Again, the EFE properties changed systematically for the samples undergo the Au-ion irradiation/annealing process with sub-critical fluence ($f < f_c$) and showed irregularly trend in EFE properties due to Au-ion irradiation with a fluence larger than $f_c = 5 \times 10^{12}$ ions/cm^2. Such a phenomenon was plotted as open triangles in Fig. 3(c).

To facilitate the comparison, the resistance of the UNCD films was measured by a 4-probe technique. It is observed that both of the pristine and Au-ion irradiated samples are very resistive, in the order of mega ohm regime. The resistance of the samples changes irregularly and is not correlated well with the fluence of Au-ion irradiated. These results show that the EFE properties are more appropriate than the 4-probe resistivities for characterizing the modifications induced by the Au-ion irradiation and the followed annealing processes. Such a phenomenon is closely related to the unique ion-to-materials reaction mechanism: the irradiated Au-ions usually induced electronic and lattice modifications on the materials preferentially along the track of incident ions that is best

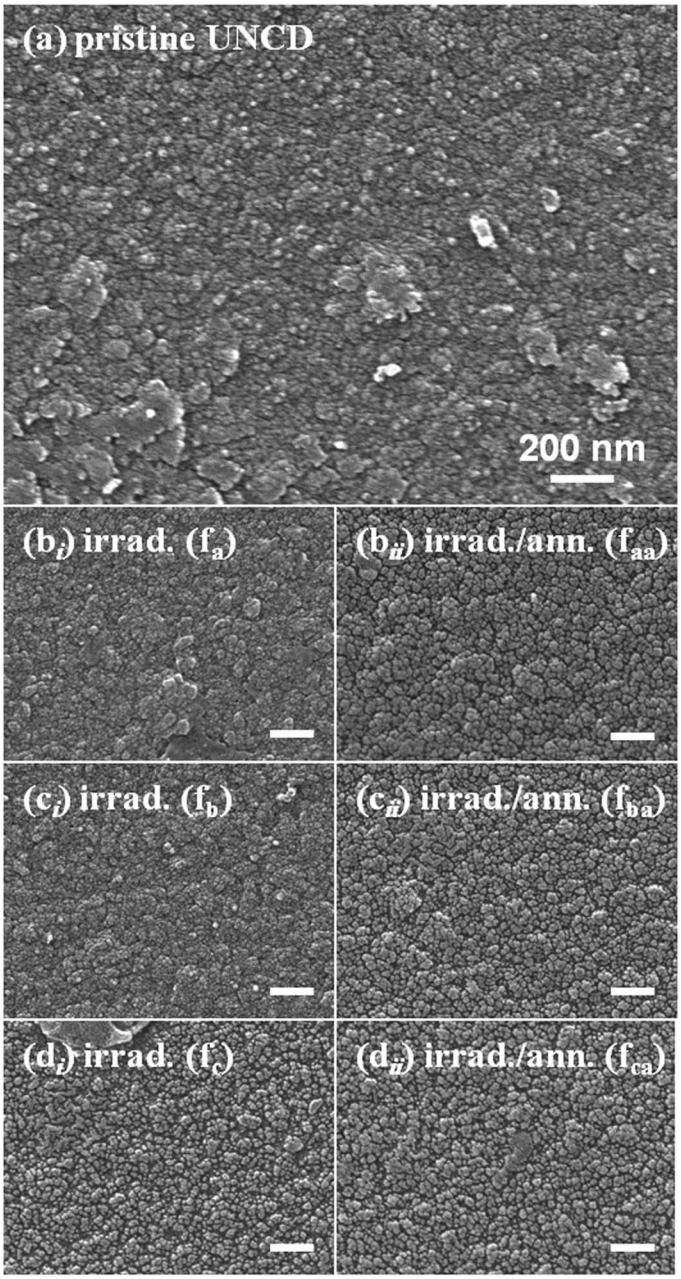

FIG. 1. The SEM micrographs of the (a) pristine UNCD films, (b_i, c_i and d_i) the Au-ion irradiated UNCD films with fluence of $f_a = 1 \times 10^{11}$ (b_i), $f_b = 1 \times 10^{12}$ (c_i), and $f_c = 5 \times 10^{12}$ (d_i) ions/cm^2 and (b_{ii}, c_{ii} and d_{ii}) the corresponding Au-ion irradiated/annealed UNCD films, i. e., with fluence of $f_{aa} = 1 \times 10^{11}$ (b_{ii}), $f_{ba} = 1 \times 10^{12}$ (c_{ii}), and $f_{ca} = 5 \times 10^{12}$ (d_{ii}) ions/cm^2 (the scale bar represents 200 nm).

demonstrated by a heavy ions irradiation effect in diamond like carbon films.[27] In these materials, the irradiation induced thermal spike may recrystallize the material locally, forming filaments of graphitic phase that provide conducting channel. The 4-probe technique for measuring the transport of electrons along the films surface cannot detect the existence of these vertically conduction channels as they are not interconnected along the films. In contrast, the EFE process is very sensitive to the presence of electron conduction channel induced by the Au-ion irradiation process, as the electrons were transported from the bottom of the Si-substrates, upward through the films and were then field emitted. Apparently, when the fluence of ion irradiation for UNCD films exceeds certain limit,

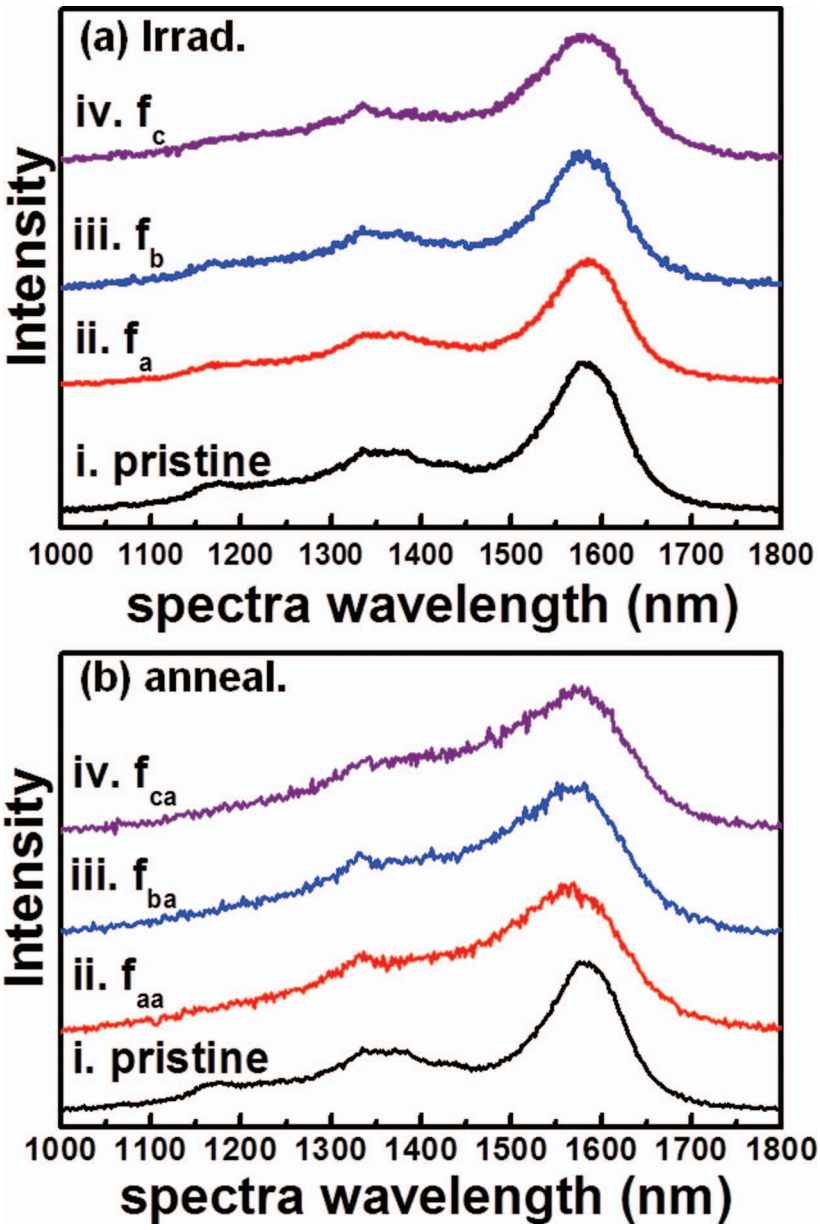

FIG. 2. The Raman spectroscopy of the (a) pristine UNCD films (*i*) and the Au-ion irradiated UNCD films with fluence of $f_a = 1 \times 10^{11}$ (*ii*), $f_b = 1 \times 10^{12}$ (*iii*), and $f_c = 5 \times 10^{12}$ (*iv*) ions/cm^2 and (b) those of the corresponding Au-ion irradiated/annealed UNCD films, i. e., with fluence of $f_{aa} = 1 \times 10^{11}$ (*ii*), $f_{ba} = 1 \times 10^{12}$ (*iii*), and $f_{ca} = 5 \times 10^{12}$ (*iv*) ions/cm^2.

substantial structural damage will be induced and results in abnormal change in EFE properties. The UNCD materials will no longer be suitable for radiation detection. Figure 3 shows that the EFE properties change irregularly for a fluence larger than $f_c = 5 \times 10^{12}$ ions/cm^2 (i.e., for samples f_c). Therefore, this fluence ($f_c = 5 \times 10^{12}$ ions/cm^2) is the high fluence limit for applying the UNCD films as radiation detectors.

The bonding structures of the diamond films that was modified by the Au-ion irradiation and irradiation/annealing processes were analyzed by NEXAFS and EELS in TEM. In Fig. 4(a) the NEXAFS spectra are presented. All the spectra contain two regimes, a prominent peak at ~285.3 eV and a relatively broad feature between ~289.5 and 302.5 eV. The former is assigned to the unoccupied π^* bond, which is characteristic of the sp^2 C=C bond.[28] The latter is due

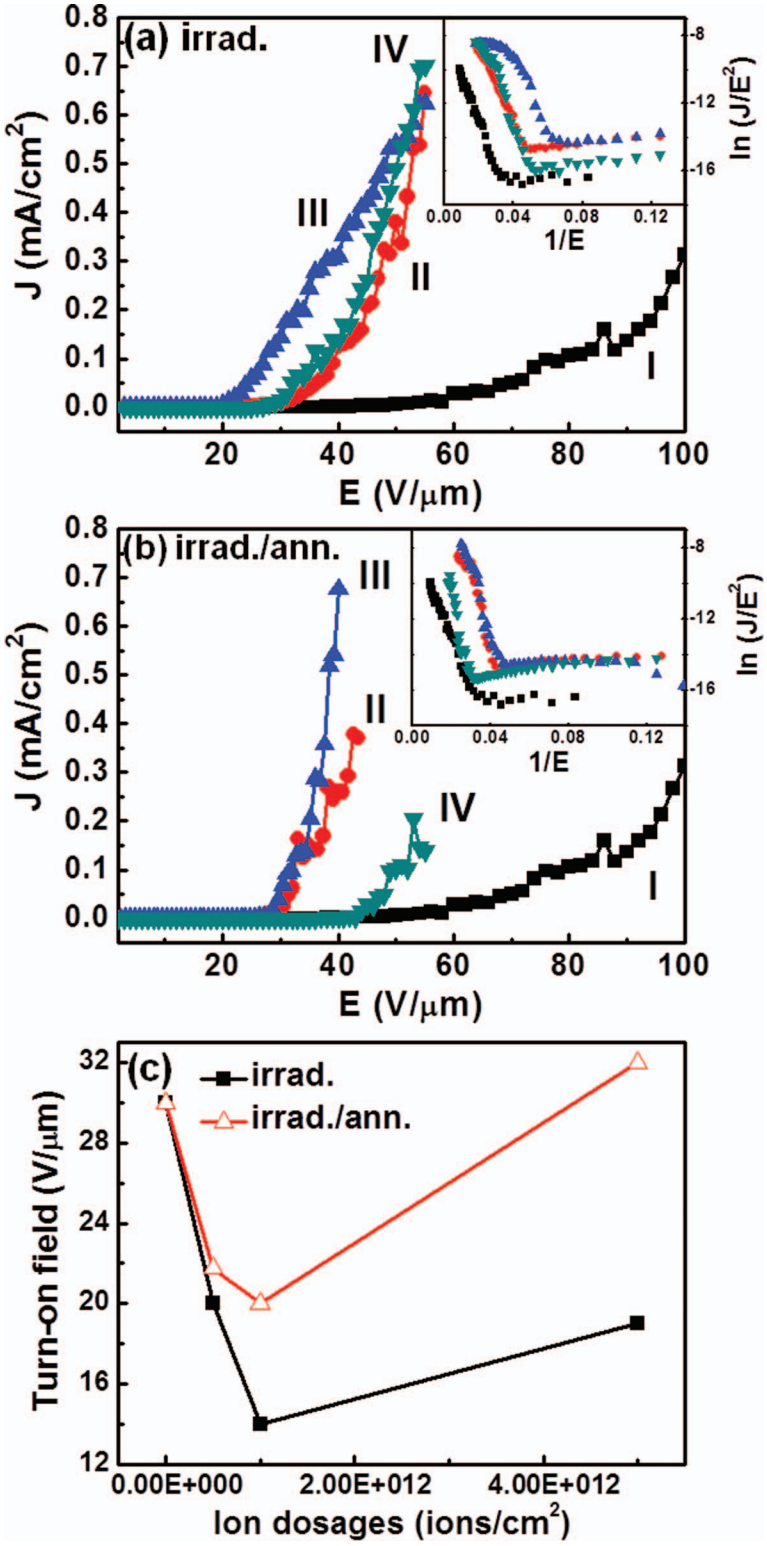

FIG. 3. The electron field emission of the (a) pristine UNCD films (*i*) and the Au-ion irradiated UNCD films with fluence of $f_a = 1 \times 10^{11}$ (*ii*), $f_b = 1 \times 10^{12}$ (*iii*), and $f_c = 5 \times 10^{12}$ (*iv*) ions/cm^2 and (b) those of the corresponding Au-ion irradiated/annealed UNCD films, i. e., with fluence of $f_{aa} = 1 \times 10^{11}$ (*ii*), $f_{ba} = 1 \times 10^{12}$ (*iii*), and $f_{ca} = 5 \times 10^{12}$ (*iv*) ions/cm^2. (c) The variation of the turn-on field versus the fluence for Au-ion irradiation (solid squares) and Au-ion irradiation/annealing (open triangles).

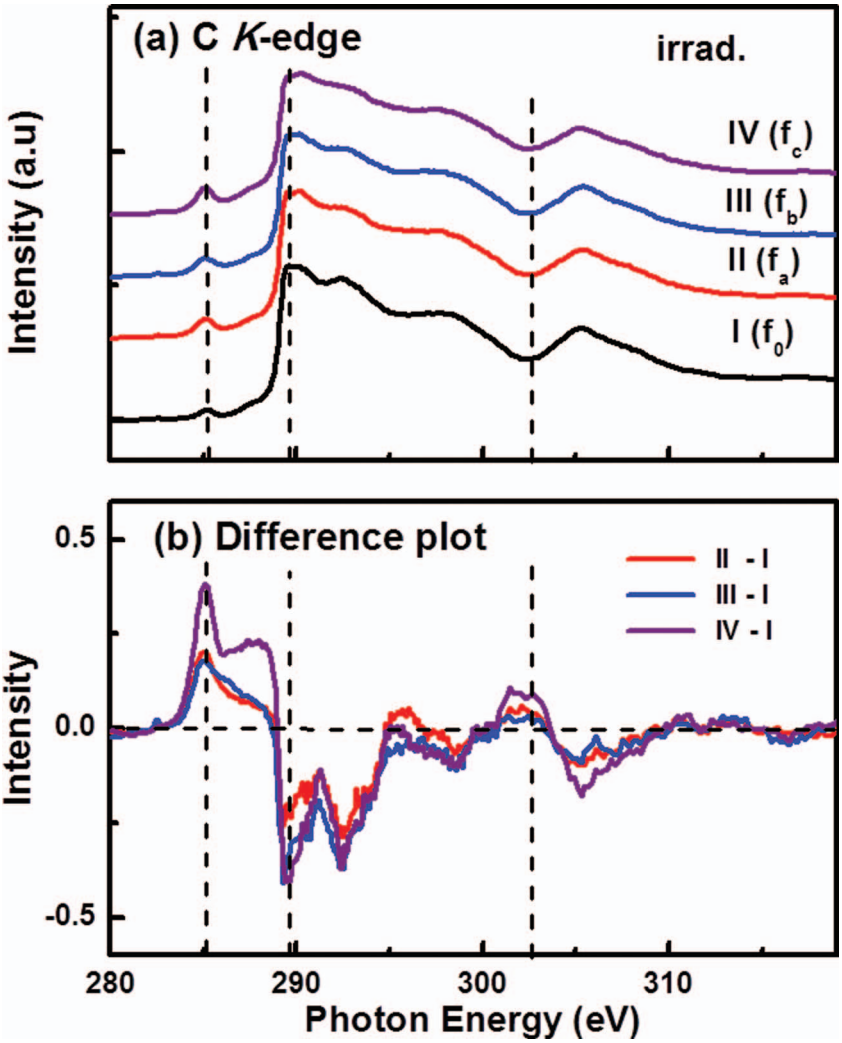

FIG. 4. (a) C *K*-edge NEXAFS of (I) pristine UNCD films and the Au-ion irradiated UNCD films with fluence of (II) $f_a = 1 \times 10^{11}$, (III) $f_b = 1 \times 10^{12}$ and (IV) $f_c = 5 \times 10^{12}$ ions/cm^2. (b) Spectral difference constructed by subtracting NEXAFS of pristine film from that of Au-ion irradiated films of different fluencies.

to σ^* bond, which is characteristic of the sp^3 tetrahedral C-C bond.[29] The peak at ~289.5 eV corresponds to the diamond core exciton, which is the result of the bound electron-hole pair.[30] The dip at ~302.5 eV, is attributed to the second absolute band gap.[31] Both are characteristics of NEXAFS spectrum corresponding to the diamond of Fd3m structure. The exciton peak and the dip are often used to evaluate the quality of diamond.[32] Also observed is a very weak bump due to C-H bond at ~287.5 eV, which is originated from the absorption of hydrocarbon to the dangling bonds at grain boundaries during the film deposition process.[33] The spectral variations due to the Au-ion irradiation can be emphasized by subtracting the spectrum of the pristine film (curve I) from the respective spectra. The difference plots are shown in Fig. 4(b). The peaks in the difference plots are the features mainly originating from the Au-ion irradiation, and the dips are the features that have been reduced by the ion irradiation. The prominent feature near 285.3 eV (π^* peak) indicates the increase of the amount of graphitic carbon contribution. The sharp dip at 289.5 eV (designated by dotted line) indicates the weakening of the exciton peak, due to the point defects created by the Au-ion irradiation.[34] The negative intensity above this dip indicates the reduced σ^* (sp^3) contribution. The positive intensity between 295 and 302 eV is due to the broad a-C contribution.[35] The peak at 302.5 eV is evidence of the significantly reduced absolute second band gap dip, which indicate

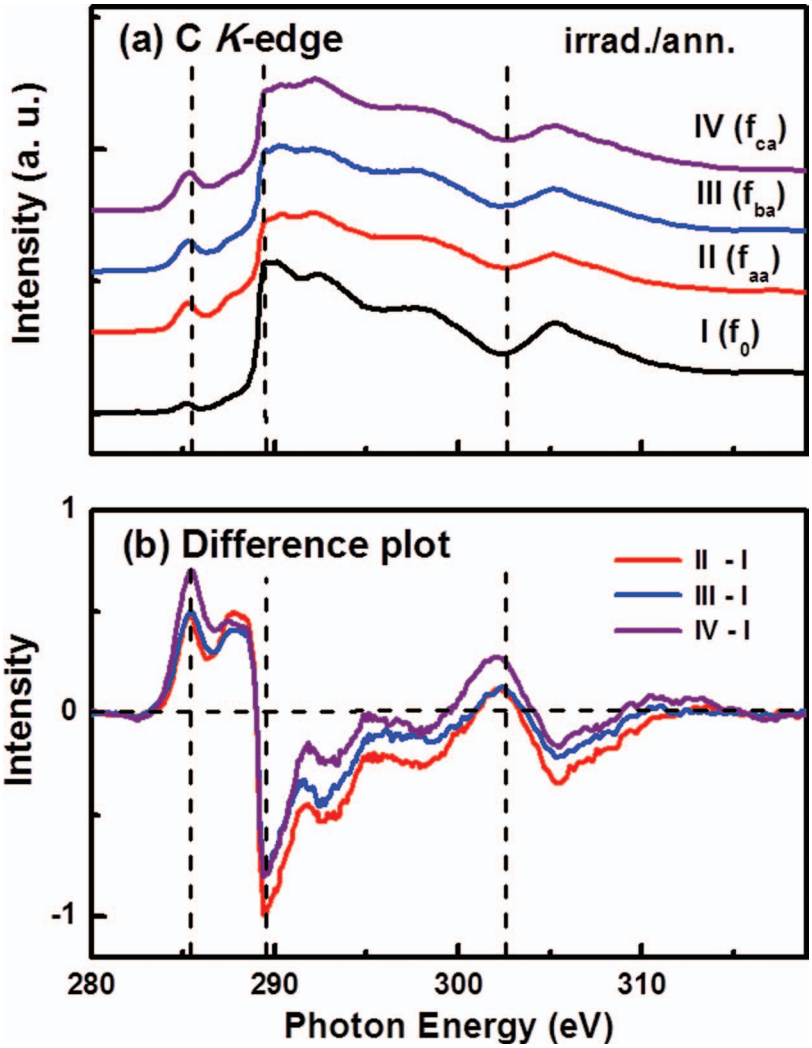

FIG. 5. (a) C *K*-edge NEXAFS of (I) pristine UNCD films and the Au-ion irradiated/annealed UNCD films with fluence of (II) $f_a = 1 \times 10^{11}$, (III) $f_b = 1 \times 10^{12}$ and (IV) $f_c = 5 \times 10^{12}$ ions/cm^2. (b) Spectral difference constructed by subtracting NEXAFS of pristine film from that of Au-ion irradiated/annealed films of different fluencies.

that the Au-ion irradiation generates defective crystalline structure in the small diamond grain.[36] The spectral changes due to the Au-ion irradiation are moderate for fluences less than critical flunce (i.e., $f_c = 5 \times 10^{12}$ ions/cm^2), while for the highest fluence (curve I_c-I) the changes are much more intense. The most dramatic change is the broad peak developed at $\sim$ 288.3 eV, which is originated from the defect induced surface states, as reported by Gago *et al*. based on the studies on ion beam damaged diamond surface.[37]

Figure 5(a) plots NEXAFS spectra of the films, which were annealed after the Au-ion irradiation. All the spectra show similar features to those in Fig. 4(a). The effect of the annealing on the Au-ion irradiated film is revealed by comparing the spectral difference relative to the pristine film, as plotted in Fig. 5(b). Similarly, two major differences are observed. First, the intensity due to a-C, between 295 and 302 eV, is reduced in addition to the dip due to the exciton peak drop. Second, the intensity of the graphite peak near 285.5 eV is enhanced while the intensity between 287 and 289 eV is obviously higher than the spectra in Fig. 4(b) indicating that the annealing has reduced the surface states and generated more C-H bonding at the surface. The amount of spectral change increases as the irradiation fluence increases.

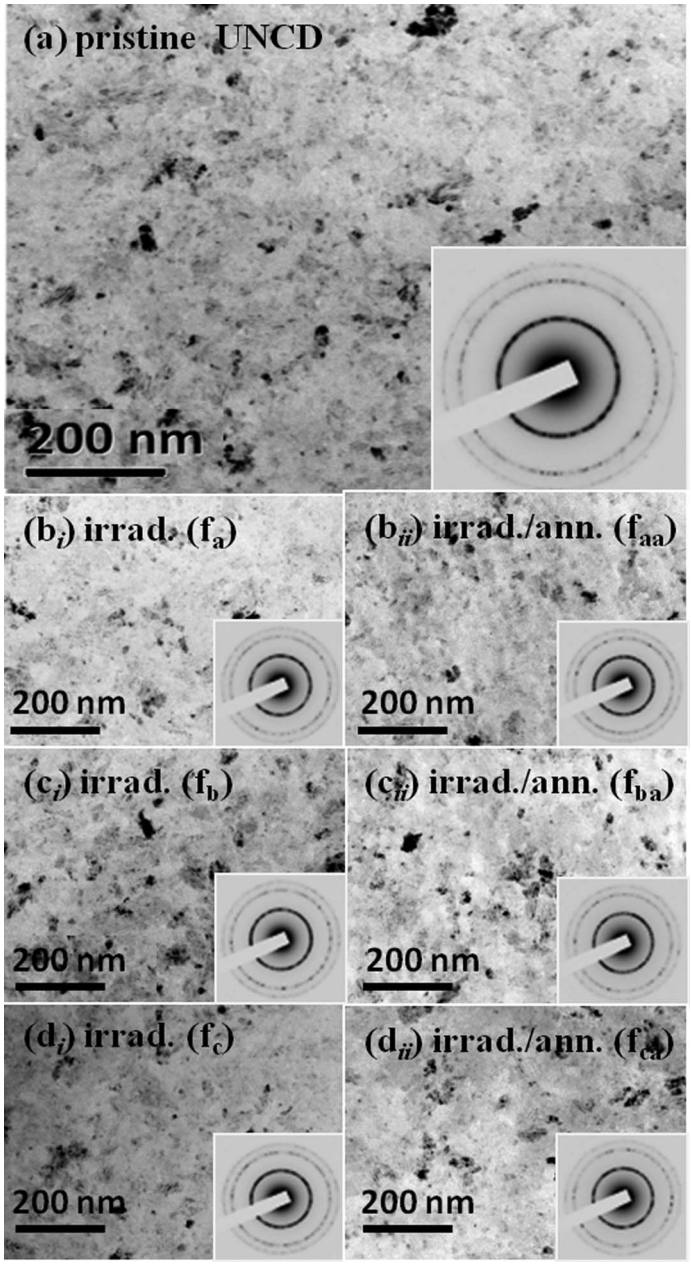

FIG. 6. The TEM micrographs of the (a) pristine UNCD films, (b_i, c_i and d_i) the Au-ion irradiated UNCD films with fluence of $f_a = 1 \times 10^{11}$ (b_i), $f_b = 1 \times 10^{12}$ (c_i), and $f_c = 5 \times 10^{12}$ (d_i) ions/cm^2 and (b_{ii}, c_{ii} and d_{ii}) the corresponding Au-ion irradiated/annealed UNCD films, i. e., with fluence of $f_{aa} = 1 \times 10^{11}$ (b_{ii}), $f_{ba} = 1 \times 10^{12}$ (c_{ii}), and $f_{ca} = 5 \times 10^{12}$ (d_{ii}) ions/cm^2 (the scale bar represents 200 nm).

B. The local Au-ion irradiation effect

While the NEXAFS provides valuable information on the modification of bonding structure for the UNCD films due to Au-ion irradiation and irradiation/annealing processes, how such processes affect the granular structure of the films locally is still not fully understood. To understand such a characteristic, the microstructure of the UNCD films was examined in detail using TEM and EELS so as to elucidate the correlation between the electrical properties and the structural change induced by the Au ion irradiation. Figure 6 shows the TEM micrographs of the pristine (Fig. 6(a)), the Au-ion irradiated (Figs. 6(b_i), 6(c_i) and 6(di)) and the irradiated/annealed (Figs. 6(b_{ii}), 6(c_{ii}) and 6(dii))

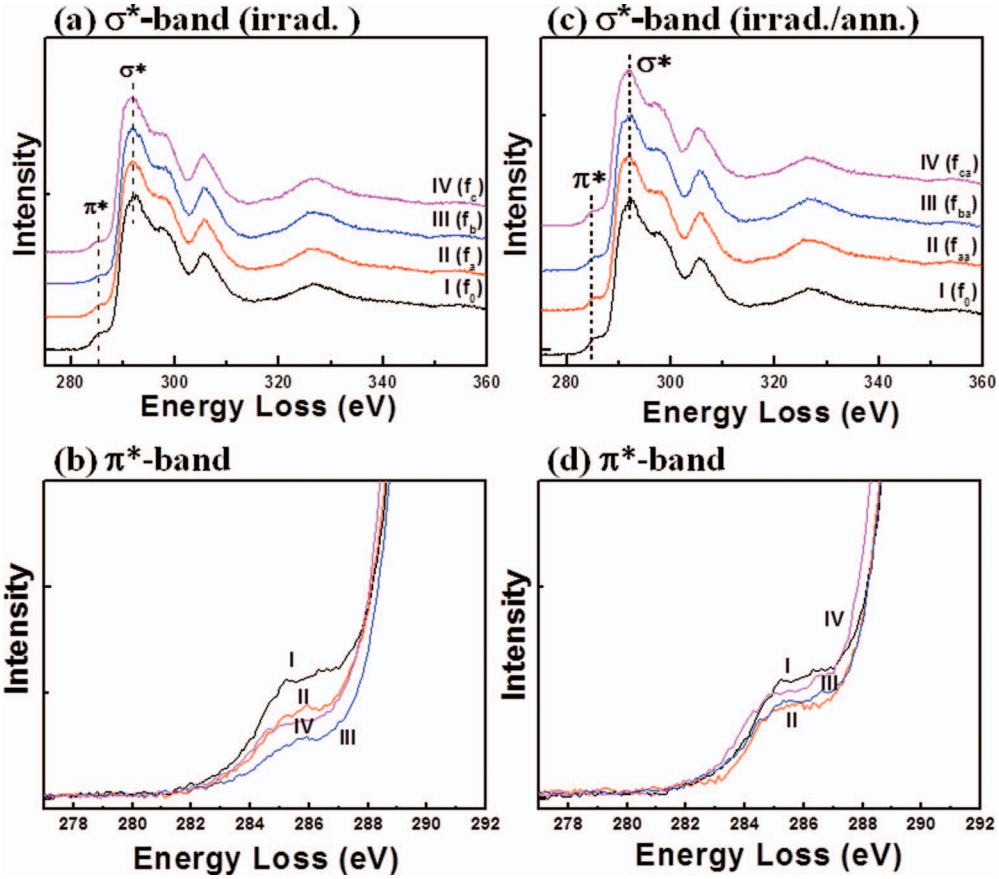

FIG. 7. The (a) carbon edge core-loss and (b) plasmon-loss EELS spectra of the pristine (*i*) and (*ii*, *iii*, *iv*) Au-ion irradiated samples with the fluence of $f_a = 1 \times 10^{11}$ (*ii*), $f_b = 1 \times 10^{12}$ (*iii*), and $f_c = 5 \times 10^{12}$ (*iv*) ions/cm^2. The (c) carbon edge core-loss and (d) plasmon-loss EELS spectra of the pristine (*i*) and (*ii*, *iii*, *iv*) Au-ion irradiated/annealed samples with the fluence of $f_a = 1 \times 10^{11}$ (*ii*), $f_b = 1 \times 10^{12}$ (*iii*), and $f_c = 5 \times 10^{12}$ (*iv*) ions/cm^2.

UNCD films. Smooth rings in the selected area electron diffraction (SAED) patterns corresponding to each TEM micrograph implies that all the UNCD films consist of ultra-small and randomly oriented diamond grains. Large diamond aggregates were observed evenly distributed among the matrix of ultra-small grains (cf. bright field images in Fig. 6). These TEM micrographs indicate that the microstructure of the UNCD films was insignificantly changed due to Au-ion irradiation for a fluence up to $f_c = 5 \times 10^{12}$ ions/cm^2.

However, Fig. 7, the selected area EELS spectra corresponding to each micrograph in Fig. 6, shows that there is some subtle change in bonding structure for these samples. The carbon edge core-loss EELS spectra shown in Figs. 7(a) and 7(c), which corresponding to Au-ion irradiated and irradiated/annealed UNCD films, respectively, indicates the presence of abrupt rise near 289.5 eV (σ^*-band) and a large dip in the vicinity of 302 eV that signifies the diamond nature of these materials.[38,39] There exists a small hump near 285 eV (π^*-band) in each EELS spectra that represents the existence of a-C phase (or C-H bond).[39] There is essentially no change in carbon edge core-loss EELS spectra due to Au-ion irradiation and irradiation/annealing processes. However, more detailed analysis by enlarging the spectra in the vicinity of π^*-band (~285 eV) for the Au-ion irradiated samples (Fig. 7(b) indicates that the π^*-band, which represents the amorphous carbon (or C-H bond) at the grain boundaries of the UNCD films,[39] decreased with the fluence of Au-ion irradiation up to sample f_b (1×10^{12} ions/cm^2, curve III). Such an observation indicates that only the C=C bonds at grain boundaries were dissociated due to Au-ion irradiation, while sp^3-bonds in the bulk of diamond grains remained intact. The curve IV in Fig. 7(b) indicates that the π^*-band

(~285 eV) reverted back to larger value when irradiated with f_c (5×10^{12} ions/cm^2), implying that the surface of the diamond grains was disrupted when the fluence of the Au-ions irradiation exceeds certain limit (i.e., $f_c = 5 \times 10^{12}$ ions/cm^2) that results in the increase in the amount of C=C bonds. Enlarged π^*-band shown in Fig. 7(d) indicates that the annealing process converted the a-C phase into more stable phases, the graphite, such that all the π^*-band approached the same value as those in pristine UNCD films.

High resolution TEM structure image and associated EELS were utilized to examine the local change in microstructure due to Au-ion irradiation. Figure 8(a) shows the plan-view, whereas Fig. 8(b) shows the cross-sectional view near diamond-to-Si interface, of the pristine UNCD films. The structure image of a typical region in pristine UNCD films (Fig. 8(a)), indicates that the diamond aggregates in the films contain parallel fringes, which are planar defects induced by coalescence process.[40] The Fourier-transformed diffractograms (FT) show that region I is predominated with crystalline materials diamond (inferred by FT_1, Fig. 8(a)) and regions II and III are predominated the non-crystalline phase (inferred by FT_2 and FT_3, Fig. 8(a)). Such characteristics were clearly illustrated by the carbon edge core-loss, π^*-bonds and plasmon-loss of the EELS spectra corresponding to the three regions (designated as solid circles in Fig. 8(a)) that are shown is Figs. 9(a_i), 9(a_{ii}) and 9(a_{iii}), respectively. The carbon edge core-loss EELS spectra in Fig. 9(a_i) show that all of the regions are predominated with diamond. It does not matter whether they were oriented along some zone axis, showing lattice fringe (region I), or off axis, showing no fringes (regions II and III). Figures 8 and 9 indicate that the EELS spectra are more appropriate technique than the TEM structural examination for revealing the bonding structure of the materials.[41] Figure 9(a_{ii}) shows that regions II and III contain slightly larger π^*-bond than the region I does, indicating the grain boundary regions (regions II and III) contained slightly larger proportion of amorphous phase (or disordered carbon). Such an observation is further supported by the plasma-loss EELS in Fig. 9(a_{iii}). Notably, the signature of the plasmon-loss EELS spectra corresponding to the diamond is a broad peak centered at 33 eV (ω_{d1}-band), which corresponds to the bulk plasmon of diamond,[42] with a prominent shoulder at 23 eV (ω_{d2}-band), which correspond to surface plasmon of diamond.[42] The peak ratio of ω_{d2} to ω_{d1} peaks is about $1{:}\sqrt{2}$. In contrast, the main feature of graphite is the peak at 27 eV (ω_g-band), which is the $\sigma+\pi$ plasmon due to all the valance electrons.[42] The plasmon-loss peak at 22 eV (ω_a-band) is less determined. It is presumably the crystal containing less density of carbon, i. e., the amorphous carbon (a-C) or *i-carbon*, the bcc structured carbon.[43] Figure 9(a_{iii}) indicates that the region I is mainly diamond, as the spectrum "1" contains mainly the bulk phasmon of diamond,[44] ω_{d1}, with large surface plasmon of diamond, ω_{d2}, as shoulder.[44] There is some graphite phase, the ω_g, existing in this region. In contrast, the region III, the periphery of diamond aggregates, is predominated with a-C phase as the spectrum 3 in Fig. 9(a_{iii}) contains large ω_a peaks, besides the bulk (ω_{d1}) and surface plamon (ω_{d2}) peaks. The region II, which is the region located in between adjacent diamond aggregates, is diamond, containing smaller proportion of a-C phase, compared with that of region III.

Cross-sectional TEM micrograph in Fig. 8(b) shows that there exists a thick layer near diamond-to-Si interface. The bonding structure of the regions near interface, which were designated as solid circles in Fig. 8(b), are shown as carbon edge core-loss EELS (Fig. 9(b_i)), silicon core-loss EELS (Fig. 9(b_{ii})) and plasma-loss EELS (Fig. 9(b_{iii})). The FT images corresponding to the regions 4 and 7 (insets 4 and 7, Fig. 8(b)), in conjunction with the EELS spectra 4 and 7 in Fig. 9(b), reveal that these regions are diamond and Si materials, respectively. The FT image (FT_5) and the associated EELS spectra (curves 5 in Figs. 9(b_i), 9(b_{ii}) and 9(b_{iii})) indicate that the interface region in diamond side (region 5, Fig. 8(b)) is the mixture of amorphous carbon and amorphous SiC. In contrast, the FT_6 and the associated EELS spectra (curve 6 in Figs. 9(b_{ii}) and 9(b_{iii})) imply that the interfacial region in Si-side (region 6, Fig. 8(b)) is Si.

The TEM and EELS investigations on f_a and f_b samples indicate that there is no apparent modification on the granular structure of UNCD films due to the moderate Au-ion irradiation with f_a and f_b fluences (figures not shown). However, when the fluence of Au-ions reaches the critical limit (f_c-value), the modification on the microstructure occurred. Figure 10(a) shows that the f_c samples possess similar granular structure with the pristine UNCD films (c.f. 8(a)), except that

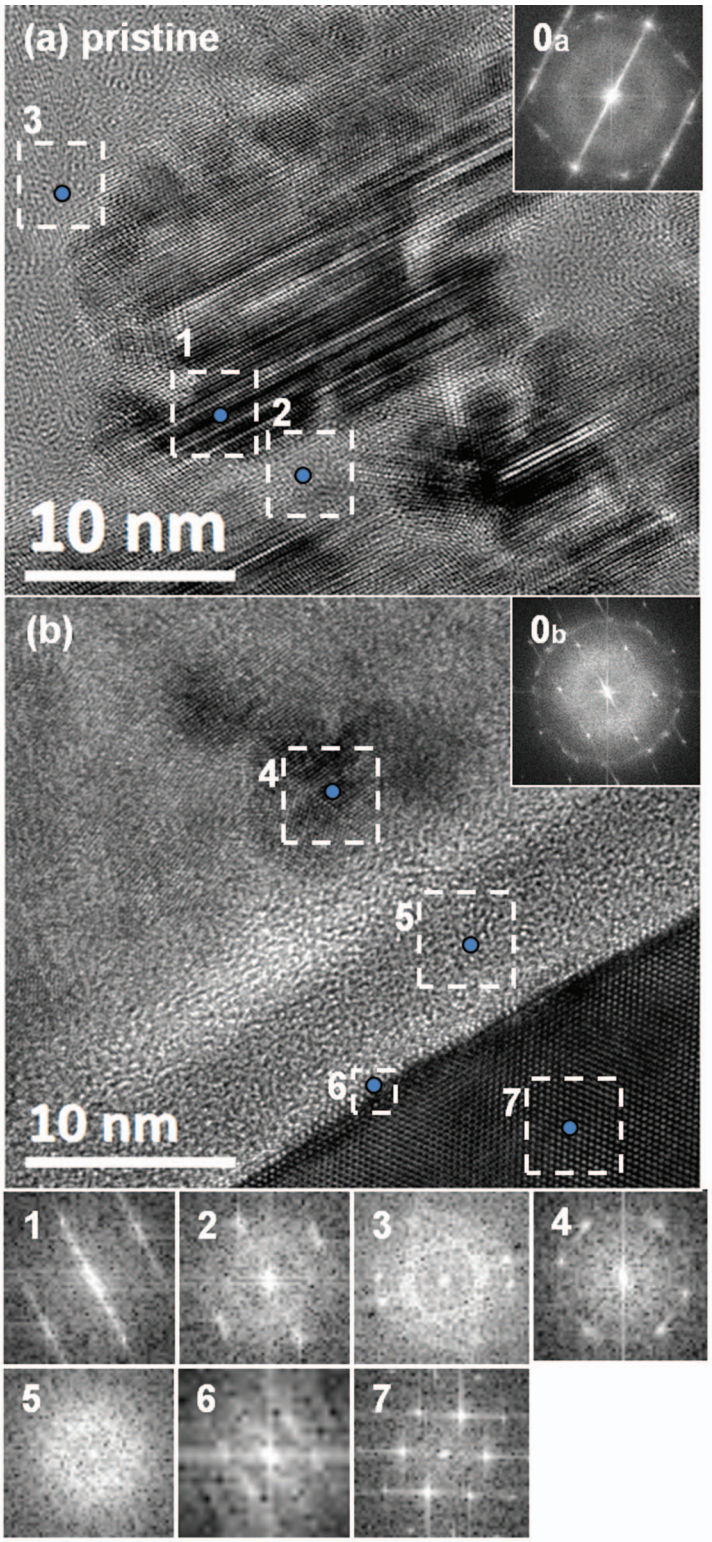

FIG. 8. The TEM structure images of (a) plan-view and (b) cross-sectional view of the pristine UNCD films. The insets 0_a and 0_b show the Fourier-transformed diffractograms corresponding to the whole structure images in "a" and "b", respectively. The FT images FT_1 to FT_7 correspond to designated regions 1 to 7, respectively.

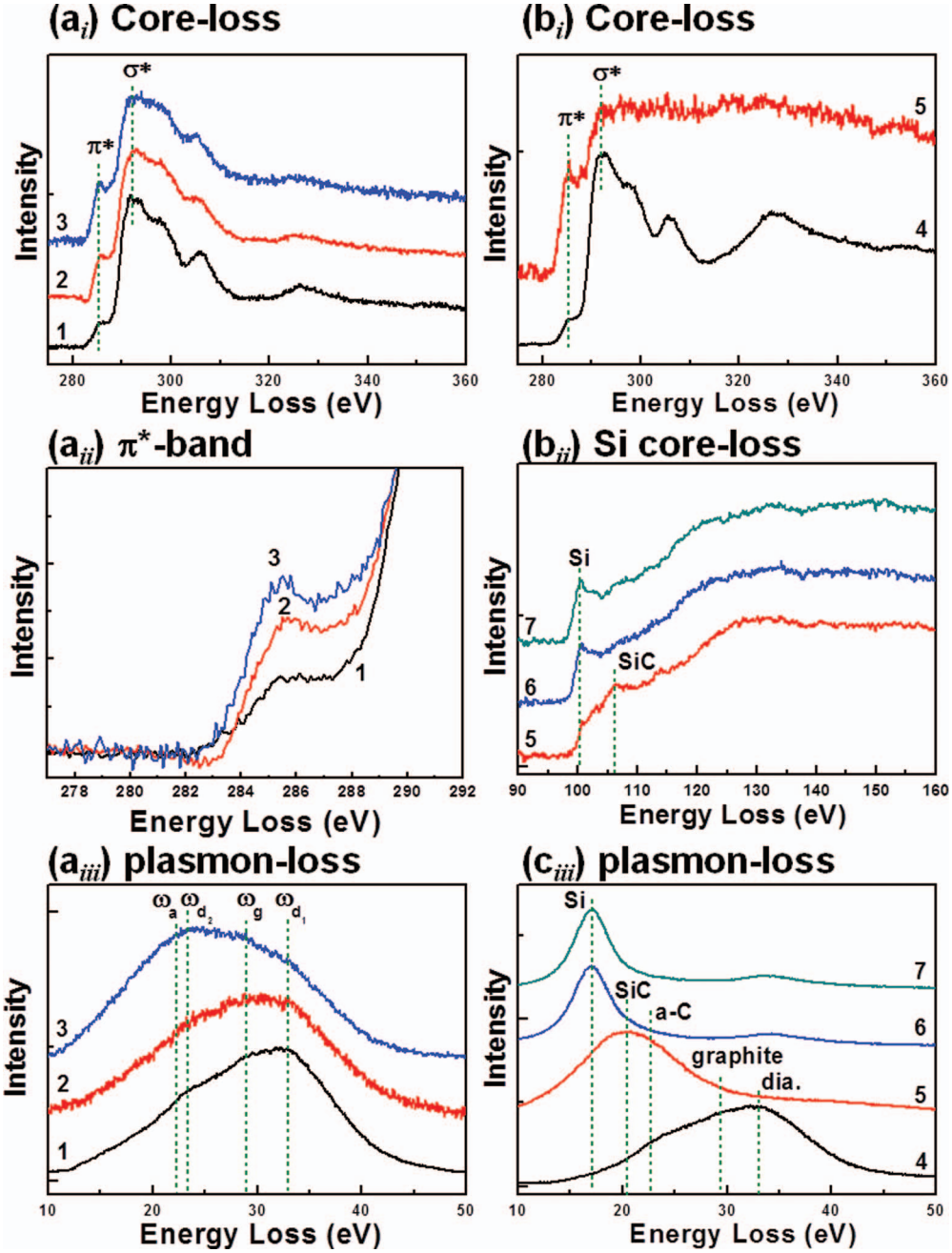

FIG. 9. The EELS corresponding to the regions in Fig. 8; (a_i) carbonedge core-loss EELS, (a_{ii}) enlarged EELS near the π^*-band and (a_{iii}) plasmon-loss EELS corresponding to the regions 1 to 3 in "a"; the (b_i) carbon edge core-loss EELS, (b_{ii}) Si edge core-loss EELS and (b_{iii}) plasmon-loss EELS corresponding to the regions 4 to 7 in "b".

the f_c samples contain more abundant aggregates and more planar defects were observed in the aggregates. Moreover, the aggregates in fc samples are hard aggregates, as they cannot be disintegrated due to electron beam irradiation. In contrast, the diamond aggregates in pristine UNCD films are soft aggregates, which are implied by the phenomenon that they are easily disintegrated due to electron beam irradiation during the TEM investigation. Moreover, there exist abundant regions with irregularities lattices (indicated by arrows, Fig. 10(a)) that are presumably resulted from the incompletely crystallization occurred in the irradiation induced coalescence process. The

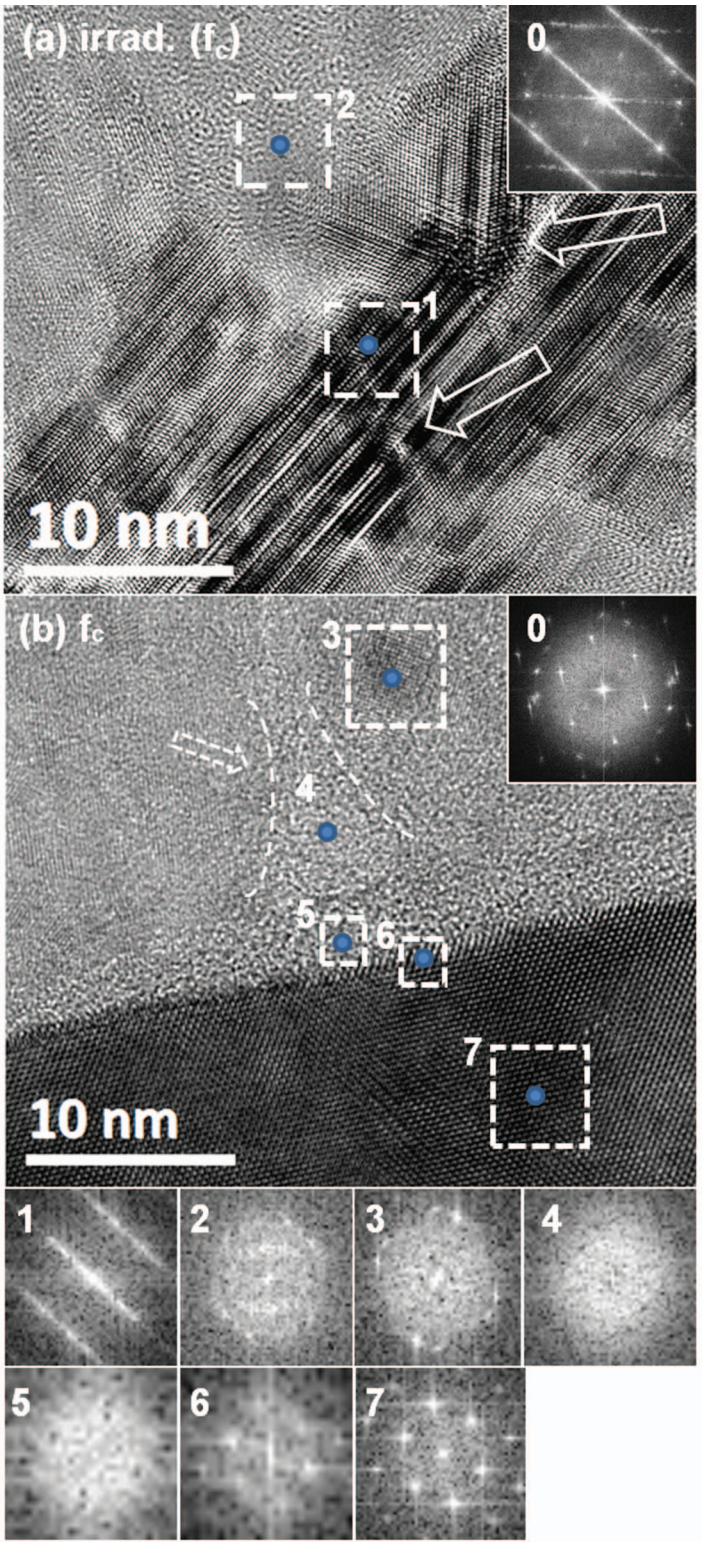

FIG. 10. The TEM structure images of (a) plan-view and (b) cross-sectional view of the UNCD films, which were irradiated with $f_c = 5 \times 10^{12}$ ions/cm^2 of Au-ions. The insets 0_a and 0_b show the Fourier-transformed diffractograms corresponding to the whole structure images in "a" and "b", respectively. The FT images FT_1 to FT_7 correspond to designated regions 1 to 7, respectively.

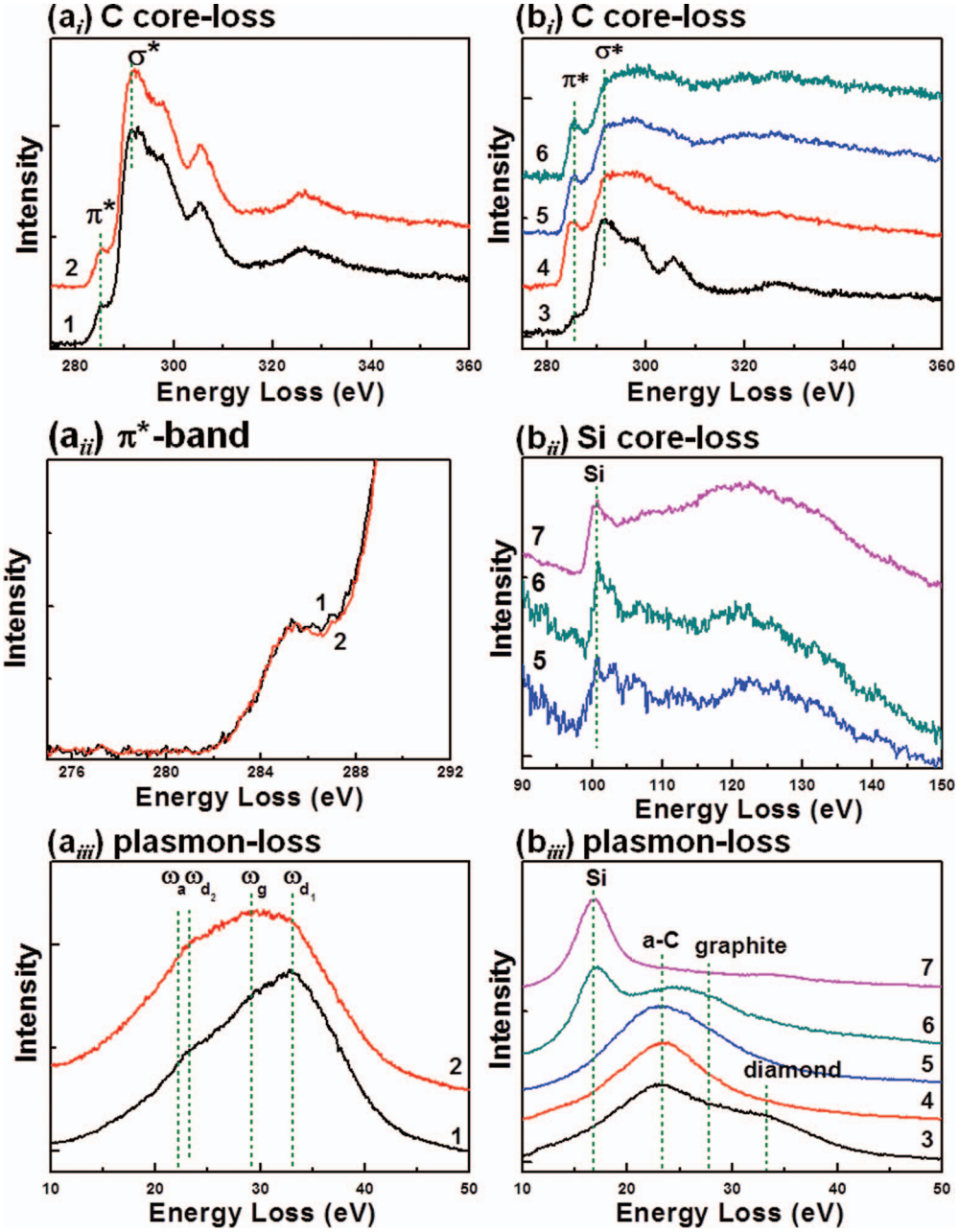

FIG. 11. The EELS corresponding to the regions in Fig. 10; (a_i) carbonedge core-loss EELS, (a_{ii}) enlarged EELS near the π^*-band and (a_{iii}) plasmon-loss EELS corresponding to the regions 1 and 2 in "a"; the (b_i) carbonedge core-loss EELS, (b_{ii}) Si edge core-loss EELS and (b_{iii}) plasmon-loss EELS corresponding to the regions 3 to 7 in "b".

associated FT images FT_1 and FT_2 indicate that the region 1 is crystalline materials (i.e., diamond) and the region 2 is non-crystalline materials, presumable, a-C phase in Fig. 10(a). However, the EELS spectra in Figs. 11(a_i) and 11(a_{ii}) show that both interior of the aggregates (region 1) and the boundaries of aggregates (region 2) are predominatly the diamond, with some proportion of a-C phase. More detailed analysis using plasmon-loss EELS (Fig. 11(a_{iii})) show, again, that both the grains (region 1) and the boundaries (region 2) are predominated with diamond as both curves 1 and 2 in Fig. 11(a_{iii}) contain ω_{d1} an ω_{d2} peaks. However, the boundaries region (region 2) contains slightly larger proportion of graphitic phase, i.e., larger ω_a and ω_g peaks in curve 2 of Fig. 11(a_{iii}).

The structure image corresponding to the interface region of f_c samples is shown in Fig. 10(b), which in conjunction with the EELS spectra in Fig. 11(b) reveals a significant change in the structure of the interfacial region due to the Au-ion irradiation with larger fluence of $f_c = 5 \times 10^{12}$ ions/cm^2. Figure 10(b) indicates that the thickness of the diamond-to-Si interface decreased markedly to about a few nanometers that are half in thickness of those in pristine UNCD films (cf. Fig. 8(b)). Moreover, besides diamond (area 3) and Si (area 7) in the respective regions, the interface was separated into two regions (areas 5 and 6). The interface in diamond-side (area 5) is also predominated with amorphous carbon (cf. core-loos EELS spectrum 5 in Fig. 11(b_i) and plasmon-loss EELS spectrum 5 Fig. 11(b_{iii})), whereas the interface in Si-side (area 6) contain both the Si and C signal (cf. core-loss EELS spectrum 6 Fig. 11(b_i) and plasmon-loss EELS spectrum 6 Fig. 11(b_{iii})), indicating that this region is the mixture of disordered carbon and amorphous SiC. Such a characteristic is different from the interfacial region in pristine UNCD films where the interface in Si-side consists of only the Si (cf. Figs. 8(b)). Interaction between Si and a-C phases was induced due to Au-ion irradiation process. Moreover, there presents a band of graphitic phase extended perpendicular to the interface toward diamond (area 4, arrowed in Fig. 10(b)). The FT image (FT_4), the corresponding core-loss EELS spectrum 4 in Fig. 11(b_i) and plasmon-loss EELS spectrum 4 in Fig. 11(b_{iii}) confirm that this area is predominated with a-C phase. It is possible that filaments of a-C phase were induced in UNCD films, which experienced Au-ion irradiation with fluence exceeds the limit value, $f_c = 5 \times 10^{12}$ ions/cm^2.

Annealing process induced the phase transformation of the Au-ion irradiated materials. The plan-view TEM structure image in Fig. 12(a) shows that the annealing process healed the structural defects contained in the diamond aggregates. No structural irregularity was observable. The corresponding carbon edge core-loss (Fig. 13(a_i)) and the plasmon-loss (Fig. 13(a_{iii})) EELS spectra indicated that although the regions "1" and "2" in Fig. 12(a) show different structure, i.e., area "1" contains fringes corresponding to diamond 111 lattice planes, whereas area "2" contains no structural feature, both regions are actually predominated with diamond (σ^*-band in Fig. 13(a_i) and $\omega_{d1} + \omega_{d2}$-band in Fig. 13($a_{iii}$)) with small proportion of amorphous phase (π^*-band in Fig. 13(a_i), ω_a- and ω_g-bands in Fig. 13(a_{iii})). The difference in structure images is arising from the fact that the area "1" is oriented near some zone-axis, whereas the area "2" is oriented away from the zone-axis. These results indicate, again, that the EELS spectroscopies are better in elucidating the nature of the bonding in these materials compared with the TEM structure investigation.

Moreover, the cross-sectional TEM structure image (Fig. 12(b)) and the corresponding EELS spectra (Fig. 13(b)) show some interesting phase transformation phenomenon. The regions 3 and 8 are, as usual, the diamond and Si (cf. spectra 3 and 8 in Figs. 13(b_i), 13(b_{ii}) and 13(b_{iii})). The interface region (diamond side) consists of two layers (areas 5 and 6). Core-loss EELS spectrum 5 in Fig. 13(b_i) and plasmon loss EELS spectrum 5 in Fig. 13(b_{iii}) indicate that the diamond-side of the interface (area 5) is predominated with carbon (mixture of a-C and graphite phases), whereas spectra 7 in Figs. 13(b_i) and 13(b_{iii}) reveal that the Si-side on interface (area 7) is predominated with crystalline SiC phase. The interface region 6 is the mixture of carbon (a-C or graphite phase) and SiC (cf. curve 6 in Figs. 13(b_i), 13(b_{ii}) and 13(b_{iii})). It should be noted that the Si-side of the interface, which was pure Si in pristine UNCD films, was converted to amorphous SiC due to Au-ion irradiation (cf. Figs. 10(b) and 11(b)) and the amorphous SiC was re-crystallized due to annealing process (cf. Figs. 12(b) and 13(b)).

Restated, when irradiated with fluence smaller than the critical value (f_a and f_b) the grain and grain boundaries of UNCD films remained intact and no structural defect was induced. Only electronic defects were induced that can modify the EFE properties for the UNCD films systematically. However, when the fluence of Au-ion irradiation approaches the critical value (e.g. $f_c = 5 \times 10^{12}$ ions/cm^2), the structural change occurred. The change in structure started at the diamond-to-Si interface, which is evidenced by the decrease in diamond-to-Si interface thickness and the induction of C-to-Si interaction (forming amorphous or crystalline SiC phase). It is believed that when the fluence of Au-ion irradiation goes beyond such a critical fluence, marked damage on the diamond lattices will occur and the electronic properties does not change systematically. Such a fluence (f_c) is the limit of detection when using UNCD films as radiation detectors.

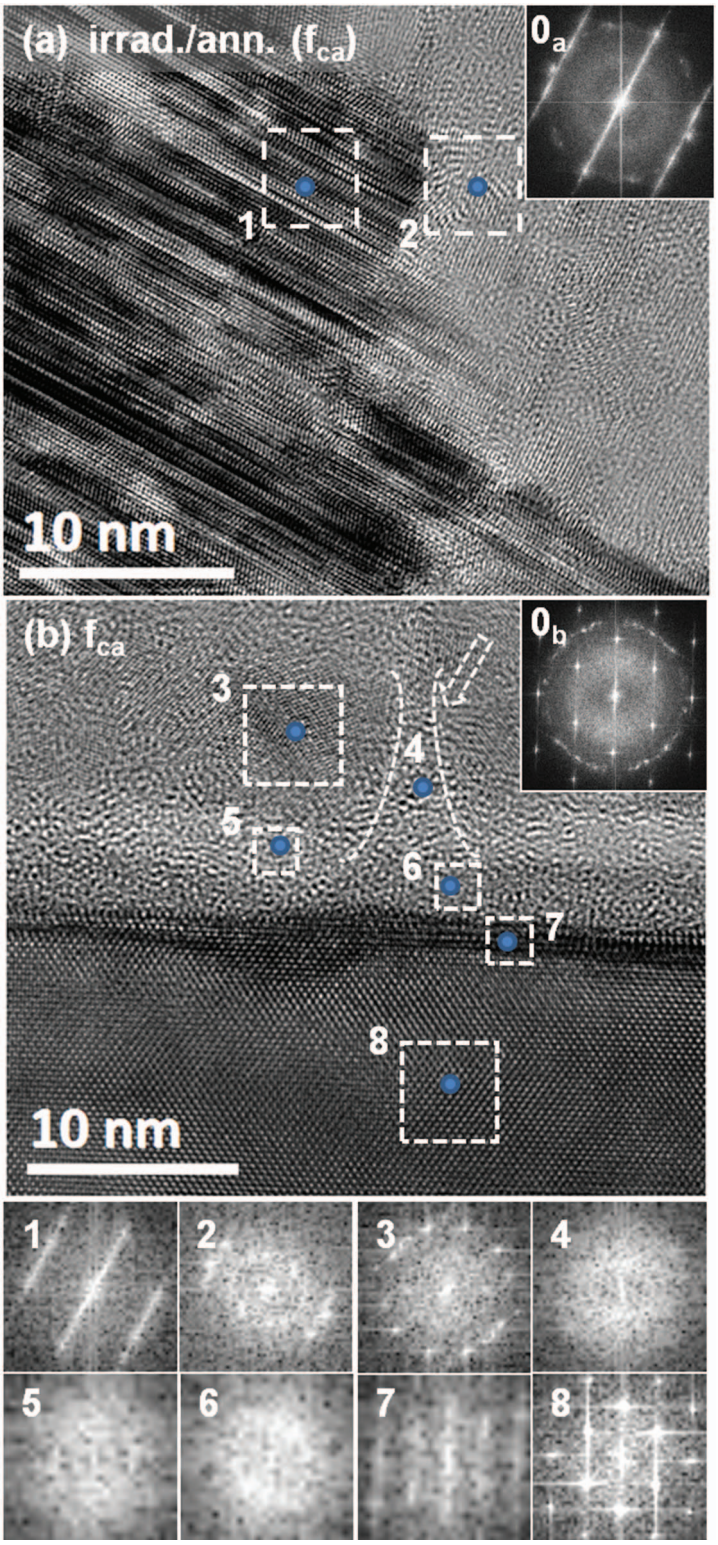

FIG. 12. The TEM structure images of (a) plan-view and (b) cross-sectional view of the annealed UNCD films, which were irradiated with $f_c = 5 \times 10^{12}$ ions/cm^2 of Au-ions. The insets 0_a and 0_b show the Fourier-transformed diffractograms corresponding to the whole structure images in "a" and "b", respectively. The FT images FT_1 to FT_7 correspond to the regions 1 to 7, respectively.

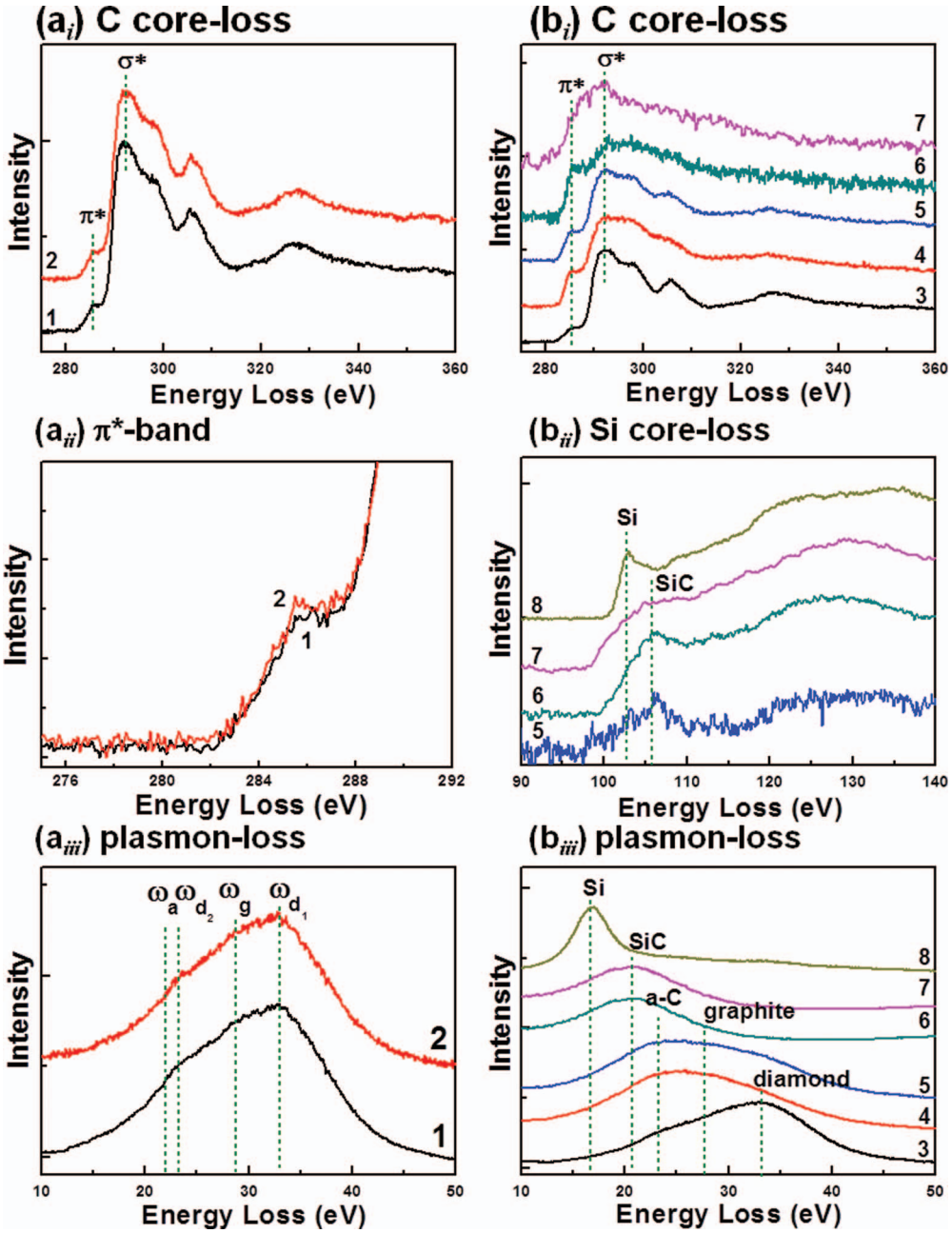

FIG. 13. The EELS corresponding to the regions in Fig. 12; (a_i) carbonedge core-loss EELS, (a_{ii}) enlarged EELS near the π^*-band and (a_{iii}) plasmon-loss EELS corresponding to the regions 1 and 2 in "a"; the (b_i) carbonedge core-loss EELS, (b_{ii}) Si edge core-loss EELS and (b_{iii}) plasmon-loss EELS corresponding to the regions 3 to 7 in "b".

IV. CONCLUSION

The potential of utilizing the UNCD films for detecting the Au-ion irradiation was investigated. When the fluence for Au-ion irradiation is lower than the critical value, $f_c = 5.0 \times 10^{12}$ ions/cm^2, the turn-on field for EFE process decreases systematically that is correlated with the increase in sp^2-bonded materials. The TEM microstructural examinations, in conjunction with EELS spectroscopic studies, reveal that the diamond-to-Si interface was preferentially modified when the fluence of Au-ion irradiation approached the critical value. The thickness of the interface decreased, the amorphous (or crystalline) SiC phase was induced. Moreover, there are a-C (or graphitic) induced

along the thickness of the films that formed electron transport tunnels and abnormally altered the EFE properties of UNCD films. These observations implied that UNCD films could be used as irradiation detectors provided that the fluence for Au-ion irradiation do not exceed the critical value. The critical fluence is the value, which will induce structural defects preferentially at UNCD-to-Si interface for the UNCD materials ($f_c = 5.0 \times 10^{12}$ ions/cm^2 in this case). When the fluence for Au-ion irradiation exceeds this critical value, the EFE processes were changed iregularly.

ACKNOWLEDGMENTS

We acknowledge Drs. Balakrishnan Sundaravel, Sankarakumar Amirthapandian, Christina Trautmann and the Materials Research Group of GSI, Darmstadt for their support during GeV irradiation at the XO beamline of the UNILAC. Financial support granted by the National Science Council of Republic of China through project Nos. NSC 101-2112-M-032-005 and NSC 101-2112-M-032-002 are gratefully acknowledged by the authors.

[1] S. F. Kozlov, E. A. Konorova, Y. A. Kuznetsov, Y. A. Salikov, V. I. Redko, V. R. Grinberg, and M. L. Meilman, IEEE TNS **24**, 235 (1977).
[2] G. Faggio, M. Marinelli, G. Messina, E. Milani, A. Paoletti, S. Santangelo, and G. V. Rinati, Microsystem Technol. **6**, 23 (1999).
[3] P. Bergonzo, A. Brambilla, D. Tromson, C. Mer, B. Guizard, F. Foulon, and V. Amosov, Diam. Relat. Mater. **10**, 631 (2001).
[4] P. Bergonzo, D. Tromson, and C. Mer, Semicond. Sci. Technol. **18**, S105–S112 (2003).
[5] Sh. Michaelson, O. Ternyak, R. Akhvlediani, A. Hoffman, A. Lafosse, R. Azria, O. A. Williams, and D. M. Gruen, J. Appl. Phys. **102**, 113516 (2007).
[6] C. J. Tang, M. A. Neto, M. J. Soares, A. J. S. Fernandes, A. J. Neves, and J. Grácio, Thin Solid Films **515**, 3539 (2007).
[7] P. Reichart, G. Datzmann, A. Hauptner, R. Hertenberger, C. Wild, and G. Dollinger, Science **306**, 1537 (2004).
[8] P. W. May, W. J. Ludlow, M. Hannaway, P. J. Heard, J. A. Smith, and K. N. Rosser, Chem. Phys. Lett. **446**, 103 (2007).
[9] K. H. Wu, E. G. Wang, Z. X. Cao, Z. L. Wang, and X. Jiang, J. Appl. Phys. **88**, 2967 (2000).
[10] S. S. Chen, H. C. Chen, W. C. Wang, C. Y. Lee, I. N. Lin, J. Guo, and C. L. Chang, J. Appl. Phys. **113**, 113704 (2013).
[11] S. M. Sze, *Physics of Semiconductor Devices* (John Wiley & Sons, 1969).
[12] D. M. Gruen, Annu. Rev. Mater. Sci. **29**, 211 (1999).
[13] J. Birrell, J. A. Carlisle, O. Auciello, D. M. Gruen, and J. M. Gibson, Appl. Phys. Lett. **81**, 2235 (2002).
[14] B. Dischler, C. Wild, W. M-Sebert, and P. Koidl, Physica B **185**, 217 (1993).
[15] S. Prawer and R. Kalish, Phys. Rev. B **51**, 15711 (1995).
[16] J. Krauser, J.-H, Zollondz, A. Weidinger, and C. Trautmann, J. Appl. Phys. **94**, 1959 (2003).
[17] N. Koenigsfeld, H. Hofsäss, D. Schwen, A. Weidinger, C. Trautmann, and R. Kalish, Diam. Relat. Mater. **12**, 469 (2003).
[18] S. Prawer, A. Hoffman, and R. Kalish, Appl. Phys. Lett. **57**, 2187 (1990).
[19] W. Zhu, G. P. Kochanski, S. Jin, L. Seibles, D. C. Jacobson, M. McCormack, and A. E. White, Appl. Phys. Lett. **67**, 1157 (1995).
[20] N. Dilawar, R. Kapil, V. D. Vankar, D. K. Avasthi, D. Kabiraj, and G. K. Mehta, Thin Solid Films **305**, 88 (1997).
[21] A. Dunlop, G. Jaskierowicz, P. M. Ossi, and S. Della-Negra, Phys. Rev. B **76**, 155403 (2007).
[22] P. T. Pandey, G. L. Sharma, D. K. Awasthi, and V. D. Vankar, Vacuum **72**, 297 (2004).
[23] P. M. Koinkar, R. S. Khairnar, S. A. Khan, R. P. Gupta, D. K. Avasthi, and M. A. More, Nucl. Instr. and Meth. B. **244**, 217 (2006).
[24] J. F. Ziegler, J. P. Biersack, and U. Littmark, *The Stopping and Ranges of Ions in Solids* (Pergamon, New York, 1985).
[25] R. H. Fowler and L. W. Nordheim, Proc. Roy. Soc. A **119**, 173 (1928)
[26] James Birrell, J. E. Gerbi, O. Auciello, J. M. Gibson, J. Johnson, and J. A. Carlisle, Diamond & Related Materials **14**, 86–92 (2005)
[27] S. Prawer, R. Kalish, M. Adel, and V. Richter, J. Appl. Phys. **61**, 4492 (1987)
[28] J. F. Morar, F. J. Himpsel, G. Hollinger, J. L. Jordon, G. Hughes, and F. R. McFeely, Phys. Rev. B **33**, 1346 (1986).
[29] J. Stöhr, *NEXAFS Spectroscopy* (Springer, New York, 1992).
[30] J. F. Morar, F. J. Himpsel, G. Hollinger, J. L. Jordon, and G. Hughes, Phys. Rev. Lett. **54**, 1960 (1985).
[31] F. L. Coffman, R. Cao, P. A. Pianetta, S. Kapoor, M. Kelly, and L. J. Terminello, Appl. Phys. Lett. **69**, 568 (1996).
[32] Y. H. Tang, X. T. Zhou, Y. F. Hu, C. S. Lee, S. T. Lee, and T. K. Sham, Chem. Phys. Lett. **372**, 320 (2003).
[33] L. Ponsonnet, C. Donnet, K. Varlot, J. M. Martin, A. Grill, and V. Patel, Thin Solid Films **319**, 97 (1998).
[34] A. Laikhtman, I. Gouzman, and A. Hoffman, Diam. Relat. Mater. **9**, 1026 (2000).
[35] R. Gago, I. Jiménez, and J. M. Albella, Surf. Sci. **482–485**, 530 (2001).
[36] L. Fayette, B. Marcus, M. Mermoux, G. Tourillon, K. Laffon, P. Parent, and F. Le Normand, Phys. Rev. B **57**, 14123 (1998).
[37] R. Gago, M. Vinnichenko, H. U. Jäger, A. Yu. Belov, I. Jiménez, N. Huang, H. Sun, and M. F. Maitz, Phys. Rev. B **72**, 014120 (2005).
[38] R. Arenal, P. Bruno, D. J. Miller, M. Bleuel, J. Lal, and D. M. Gruen, Phys. Rev. B **75**, 195431 (2007).
[39] Dieter M. Gruen, Shengzhong Liu, Alan R. Krauss, Jianshu Luo, and Xianzheng Pan, Appl. Phys. Lett. **64** (12), 1502 (1994).
[40] C. S. Wang, H. C. Chen, H. F. Cheng, and I. N. Lin, J. Appl. Phys. **107**, 034304 (2010).

[41] Ying-Gang Lu, Stuart Turner, Johan Verbeeck, Stoffel D. Janssens, Patrick Wagner, Ken Haenen, and Gustaaf Van Tendeloo, Appl. Phys. Lett. **101**, 041907 (2012).
[42] P. Kovarik, E. B. D. Bourdon, and R. H. Prince, Phys. Rev. B **48**, 12123 (1993).
[43] S. Prawer, J. L. Peng, J. O. Orwa, J. C. McCallum, D. N. Jamieson, and L. A. Bursill, Phys. Rev. B **62**, R16360 (2000).
[44] S. Prawer, K. W. Nugent, D. N. Jamieson, J. O. Orwa, L. A. Bursill, and J. L. Peng, Chemical Physics Letters **332**, 93 (2000).